








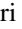

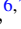




## Competing anisotropies in the chiral cubic magnet $\text{Co}_8\text{Zn}_8\text{Mn}_4$ unveiled by resonant x-ray magnetic scattering

Victor Ukleev <sup>1,\*</sup>, Oleg I. Utesov <sup>2</sup>, Chen Luo <sup>1</sup>, Florin Radu <sup>1</sup>, Sebastian Wintz <sup>1</sup>, Markus Weigand <sup>1</sup>, Simone Finizio <sup>1,3</sup>, Moritz Winter <sup>4,5</sup>, Alexander Tahn <sup>5</sup>, Bernd Rellinghaus <sup>5</sup>, Kosuke Karube <sup>6</sup>, Yoshinori Tokura <sup>6,7,8</sup>, Yasujiro Taguchi <sup>6</sup> and Jonathan S. White <sup>9</sup>

<sup>1</sup>*Helmholtz-Zentrum Berlin für Materialien und Energie, D-14109 Berlin, Germany*

<sup>2</sup>*Center for Theoretical Physics of Complex Systems, Institute for Basic Science, Daejeon 34126, Republic of Korea*

<sup>3</sup>*Swiss Light Source, Paul Scherrer Institute, CH-5232 Villigen PSI, Switzerland*

<sup>4</sup>*Max Planck Institute for Chemical Physics of Solids, D-01187 Dresden, Germany*

<sup>5</sup>*Dresden Center for Nanoanalysis, cfaed, Technical University Dresden, D-01069 Dresden, Germany*

<sup>6</sup>*RIKEN Center for Emergent Matter Science (CEMS), Wako 351-0198, Japan*

<sup>7</sup>*Department of Applied Physics, University of Tokyo, Tokyo 113-8656, Japan*

<sup>8</sup>*Tokyo College, University of Tokyo, Tokyo 113-8656, Japan*

<sup>9</sup>*Laboratory for Neutron Scattering and Imaging (LNS), Paul Scherrer Institute (PSI), CH-5232 Villigen, Switzerland*



(Received 14 March 2024; revised 20 April 2024; accepted 22 April 2024; published 8 May 2024)

The cubic  $\beta$ -Mn-type alloy  $\text{Co}_8\text{Zn}_8\text{Mn}_4$  is a chiral helimagnet that exhibits a peculiar temperature-dependent behavior in the spiral pitch, which decreases from 130 nm at room temperature to 70 nm below 20 K. Notably, this shortening is also accompanied by a structural transition of the metastable skyrmion texture, transforming from a hexagonal lattice to a square lattice of elongated skyrmions. The underlying mechanism of these transformations remains unknown, with interactions potentially involved including the temperature-dependent Dzyaloshinskii-Moriya interaction, magnetocrystalline anisotropy, and exchange anisotropy. Here, x-ray resonant magnetic small-angle scattering in vectorial magnetic fields was employed to investigate the temperature dependence of the anisotropic properties of the helical phase in  $\text{Co}_8\text{Zn}_8\text{Mn}_4$ . Our results reveal quantitatively that the magnitude of the anisotropic exchange interaction increases by a factor of 4 on cooling from room temperature to 20 K, leading to a 5% variation in the helical pitch within the (001) plane at 20 K. While the anisotropic exchange interaction contributes to the shortening of the spiral pitch, its magnitude is insufficient to explain the variation in the spiral periodicity from room to low temperatures. Finally, we demonstrate that magnetocrystalline and exchange anisotropies compete, with each favoring different orientations of the helical vector in the ground state.

DOI: [10.1103/PhysRevB.109.184415](https://doi.org/10.1103/PhysRevB.109.184415)

### I. INTRODUCTION

In recent years, there has been significant interest in the investigation of particle-like magnetic solitons, primarily due to their potential use as fundamental building blocks for spintronic devices [1–3]. These intriguing textures include chiral solitons [4] and topologically nontrivial spin hedgehogs [5] and skyrmions [3,6,7], which are known to give rise to emergent electromagnetic phenomena essential for the advancement of dissipationless electronics and next-generation technologies [2,3]. A key aspect in comprehending and harnessing these magnetic structures lies in the exploration of their manifestation in noncentrosymmetric magnetic materials, which offer a fertile ground for the formation of various twisted spin textures [8].

In cubic chiral magnets, a rich variety of modulated magnetic states arises from the competition between several fundamental interactions, such as the Heisenberg ex-

change interaction, the antisymmetric Dzyaloshinskii-Moriya interaction (DMI), the anisotropic exchange interaction (AEI), and cubic anisotropy [9–14]. Recently, a new family of chiral cubic Co-Zn-Mn intermetallics with tunable magnetic properties has been discovered [15]. These materials crystallize in the  $\beta$ -Mn-type structure and exhibit rich magnetic phase diagrams that vary in their structure according to the precise composition [16]. Moreover, in addition to the generally complex landscape of magnetic interactions, the effects of magnetic frustration and of both structural and magnetic disorder also play crucial roles in the phase diagram of these compounds [16–27].

$\text{Co}_8\text{Zn}_8\text{Mn}_4$  sustains particular attention because it hosts an equilibrium skyrmion lattice phase at room temperature under moderate magnetic fields [17]. Intriguingly, for  $\text{Co}_8\text{Zn}_8\text{Mn}_4$  as well as for similar compounds with different Mn concentrations, the helical spiral period  $\lambda$  is observed to decrease significantly as the temperature decreases, leading to a substantial increase in the spiral wave vector  $Q_0 = 2\pi/\lambda \sim D/J$ , where  $D$  is the DMI constant and  $J$  is the exchange stiffness [16]. In  $\text{Co}_8\text{Zn}_8\text{Mn}_4$  for example, the increase of the

\*victor.ukleev@helmholtz-berlin.de

helical wave vector by  $\sim 50\%$  on cooling from 300 K to below 20 K affects the structural properties of either equilibrium helical or metastable skyrmion lattice states, and plays a key role in the transition between different high- and low-temperature metastable skyrmion lattice coordinations [17,28–30].

The role of anisotropic interactions, including cubic and exchange anisotropies, has been extensively studied in the context of how they determine the properties of chiral magnets [13,14,31,32]. Specifically, the competition between these two interactions significantly affects macroscopic parameters such as the transition magnetic fields between different magnetic states [12,32,33]. However, disentangling their contributions through direct experimental observations is challenging, since both interactions can simultaneously influence the macroscopic observables. Even neutron scattering techniques, which provide microscopic information about materials, often require additional theoretical models to distinguish between the contributions of cubic and exchange anisotropies. Therefore, a comprehensive investigation of the interplay between these interactions in chiral magnets is needed for a complete understanding of their magnetic phase diagrams and how to exploit these exotic magnetic phases for applications.

To gain a deeper understanding of the microscopic magnetic interactions in  $\text{Co}_8\text{Zn}_8\text{Mn}_4$ , it is essential to probe them independently, without relying on indirectly related parameters. Recently, the temperature dependence of both the magnetocrystalline anisotropies [24] and the exchange stiffness [34] have been quantified by means of ferromagnetic resonance and neutron spectroscopy, respectively. From the latter study, it was suggested that besides an increase in the exchange stiffness at low temperature, a quantitatively accurate description of the size of the observed spiral wave vector elongation requires a further concomitant variation on cooling of other interactions involved, such as an increase in the DMI constant.

In this study, we report direct measurements of the anisotropic exchange interaction (AEI) in  $\text{Co}_8\text{Zn}_8\text{Mn}_4$  using resonant elastic small-angle x-ray scattering [35]. Through the investigation of the temperature dependence of the AEI constant, we successfully parametrize a further fundamental interaction that participates in the unusual temperature variation of the helical wave vector and the transformation of the metastable skyrmion lattice. We discuss the results within the context of composition-tuning of competing anisotropies in Co-Zn-Mn compounds as a means to gain control over the observable helical structures in these materials.

## II. EXPERIMENTAL

The single crystal of  $\text{Co}_8\text{Zn}_8\text{Mn}_4$  used for resonant elastic soft x-ray scattering (REXS) experiments was grown using the Bridgman method, as described in Ref. [17]. From the oriented bulk specimen, a  $\text{Co}_8\text{Zn}_8\text{Mn}_4$  lamella with a thickness of approximately 190 nm and an area of approximately  $10 \times 10 \mu\text{m}^2$  was cut parallel to the (100) plane and subsequently thinned using a focused ion beam system (FIB). To facilitate the experiments, the lamella was attached to a gold-coated  $\text{Si}_3\text{N}_4$  membrane (Silson Ltd., UK) using four Pt contacts deposited by FIB. Before attaching the lamella,

a circular aperture with an 8  $\mu\text{m}$  diameter was milled through the membrane and the gold layer to allow x-ray transmission through the sample. A scanning electron microscopy (SEM) image of the sample is shown in Fig. 1(a). For more comprehensive details about the sample fabrication routine, we refer to Ref. [29]. More details on the sample synthesis, characterization, and nanofabrication are given in the Supplemental Material [36].

The  $\text{Co}_8\text{Zn}_8\text{Mn}_4$  sample, mounted on the membrane, was placed onto a Cu sample holder and loaded into the vector-field cryomagnet VEK MAG at the PM-2 beamline [37] at BESSY II, Helmholtz-Zentrum Berlin, Germany. Note that the in-plane orientation of the sample with respect to the laboratory frame of reference was chosen arbitrarily.

Circularly polarized soft x-ray beams were utilized at an energy tuned to the Co  $L_3$  edge ( $E = 775.8$  eV), where the intensity of magnetic satellites reached its maximum. The sample was then cooled down in the absence of a magnetic field to a temperature of 20 K, which is a few degrees above the spin-glass transition [16,23]. The details of the small-angle REXS experiment in a vector field closely matched those reported in Refs. [35,38]. The charge-coupled device (CCD) detector ALEX-i 4k4k with  $4096 \times 4096$  pixels<sup>2</sup> (GreatEyes GmbH, Berlin, Germany) was employed, allowing an accessible range of scattering angles  $2\theta$  of  $\pm 3^\circ$ . Since the detector pixel size ( $15 \mu\text{m} \times 15 \mu\text{m}$ ) did not limit the resolution in this particular experiment, a hardware binning of 2 was utilized for faster image acquisition. The typical acquisition time for each small-angle scattering pattern was 30 seconds.

## III. RESULTS AND DISCUSSION

After zero-field cooling, the helical propagation vector in the (001) plane of the  $\text{Co}_8\text{Zn}_8\text{Mn}_4$  crystal was determined using a vector magnetic field training procedure. This procedure involves saturating the sample with a vectorial magnetic field of 150 mT applied at an angle  $\theta$  in the sample plane. Here,  $\theta = 0^\circ$  corresponds to the vertical direction  $\mathbf{z}$  in the laboratory frame of reference. Subsequently, the magnetic field was gradually reduced to zero. Similar to the case of FeGe [35], this training procedure results in the alignment of the spiral propagation vector at any  $\theta$  angle in the sample plane [see Fig. 1(b)]. To map out the period of the spiral as a function of the propagation direction in the (001) plane, measurements were carried out with  $\theta$  steps of  $3^\circ$ , covering a temperature range from 20 K to 275 K. Two-dimensional REXS patterns obtained at 50 K by summing up measurements over all azimuthal magnetic field training angles ( $\theta = 0 \dots 180^\circ$ ) with a  $3^\circ$  step are shown in Fig. 1(c). The field training procedure was working successfully for all measured temperatures and magnetic field angles in the (001) plane.

As a demonstration of the field training procedure, we show a reciprocal [Fig. 2(a)] and real space image [Fig. 2(b)] of the resulting magnetic helical structure, measured at 200 K. At this temperature the magnitude of the spiral wave vector is approximately 1.5 times larger than at 50 K. The real-space image of the aligned helical texture in the same sample was obtained using scanning transmission x-ray microscopy (STXM) at the Co  $L_3$  edge with the MAXYMUS instrument

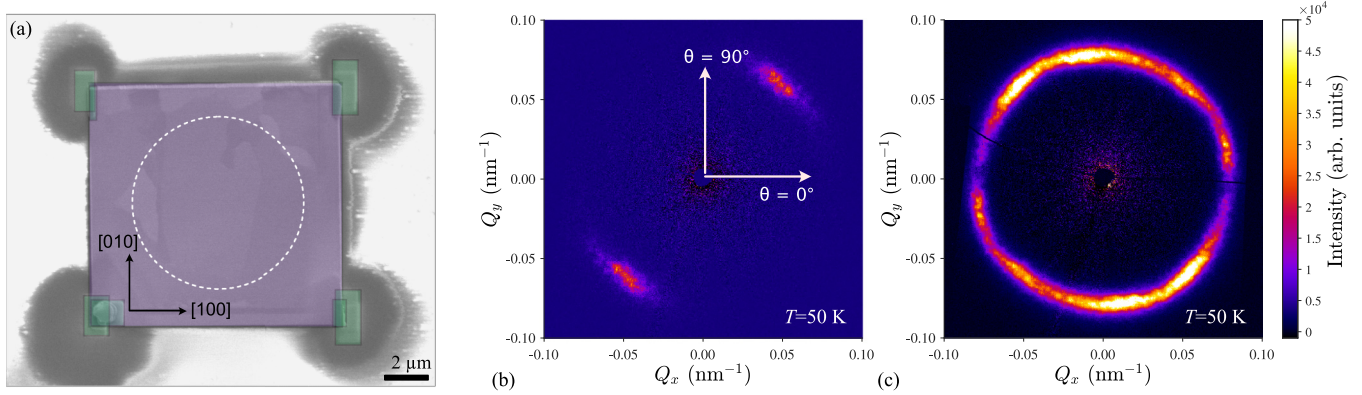


FIG. 1. (a) SEM image of the (001)  $\text{Co}_8\text{Zn}_8\text{Mn}_4$  thin plate (purple color) attached to a  $\text{Si}_3\text{N}_4$  membrane by Pt contacts (green). The circular aperture drilled in the gold layer on the back side of the membrane is shown as a dashed line. (b) Zero-field REXS pattern measured at  $T = 50$  K after the field training  $\mu_0 H = 0.12$  T applied at  $\theta = 45^\circ$ . (c) REXS patterns measured at 50 K summed up over all azimuthal magnetic field training angles  $\theta = 0 \dots 180^\circ$  with a  $3^\circ$  step.

at BESSY II [39] [Fig. 2(b)], operated by the Helmholtz-Zentrum für Materialien und Energie.

The REXS patterns obtained for each temperature and azimuthal magnetic field training angle  $\theta$  show a pair of Bragg peaks corresponding to the helical texture aligned in the corresponding in-plane direction. In Figs. 3(a)–3(g), we present the temperature dependence of the extracted peak positions  $Q(\theta)$ . At low temperatures ( $T \leq 150$  K), the dependence clearly exhibits a fourfold character, as expected for the cubic symmetry in the (001) plane [12].

The spiral wave vector  $Q$  in the (001) plane reaches a local maximum (corresponding to a minimum real-space period  $\lambda$ ) when aligned along [110]-equivalent crystal axes and a minimum when aligned along [100] directions. At 20 K, the magnitude of the  $Q$ -vector oscillation in the (001) plane reaches approximately 5%. This general behavior of the helical wave vector directly provides the sign of the AEI constant  $F$  to be negative, similar to both MnSi [40] and  $\text{Cu}_2\text{OSeO}_3$  [38,41], which in principle is expected to favor a preferred alignment of helical wave vectors along the

body diagonals of the cubic lattice  $\langle 111 \rangle$  [12].  $\text{Co}_8\text{Zn}_8\text{Mn}_4$  is known to display a preferred alignment of the helical wave vectors with the cubic  $\langle 100 \rangle$  axes at all temperatures [16,17], consistent in principle with a positive value of  $F$ . The negative sign of  $F$  found experimentally here therefore implies a competition between the different helical wave vector alignment tendencies promoted by a predominant cubic anisotropy [24] favoring the observed  $\langle 100 \rangle$  directions, and the weaker AEI. A similar situation was recently observed in  $\text{Cu}_2\text{OSeO}_3$  [38], where the interplay of frustrated anisotropies stabilizes exotic tilted conical and disordered skyrmion phases at low temperatures when a magnetic field is applied along [001].

Upon elevating the temperature above 20 K, the  $Q(\theta)$  dependence becomes more isotropic (Fig. 3). At around  $T \sim 200$  K and above, the fourfold feature is no longer pronounced, but the distribution is not completely isotropic either. Instead, a weak uniaxial distortion of  $Q(\theta)$  is observed that can be successfully explained by considering an effect of spiral distortion induced by uniaxial tensile strain [38,42]. To

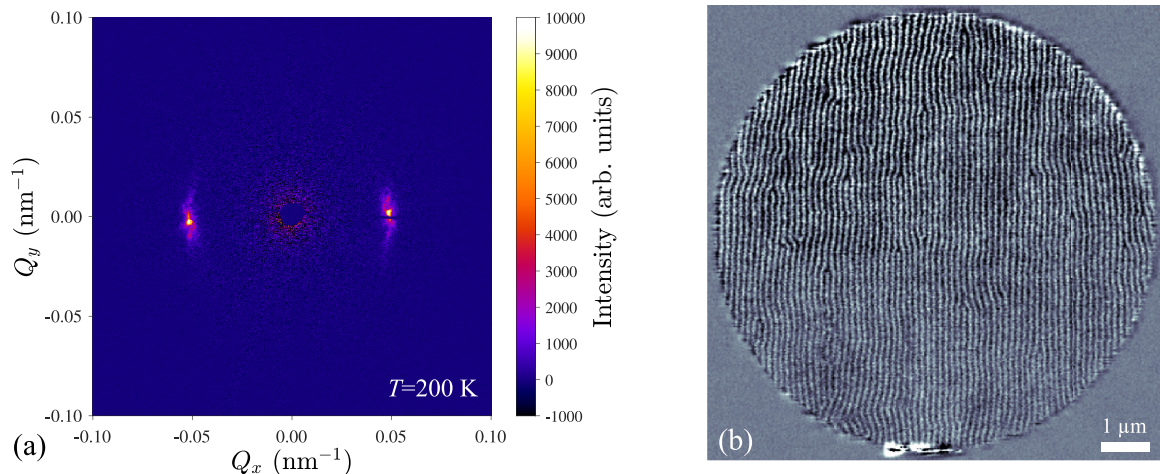


FIG. 2. (a) Zero-field REXS pattern measured at  $T = 200$  K after the field training  $\mu_0 H = 0.12$  T applied at  $\theta = 0^\circ$ . (b) SXTM image of the aligned helical texture at  $T = 200$  K obtained using circularly polarized x rays, which are sensitive to the out-of-plane component of magnetization.

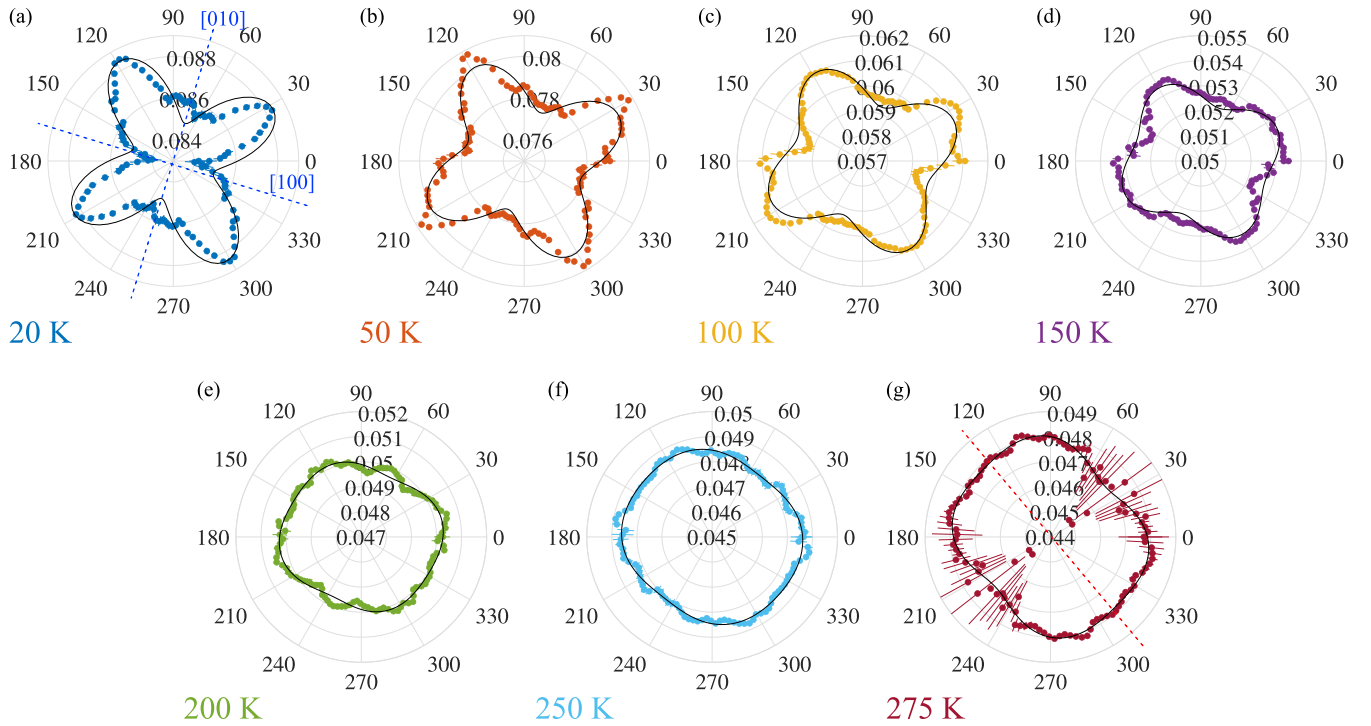


FIG. 3. Polar plots of the helical wave vector magnitude  $Q$  in  $\text{nm}^{-1}$  units as a function of azimuthal angle  $\theta$  at (a) 20 K, (b) 50 K, (c) 100 K, (d) 150 K, (e) 200 K, (f) 250 K, (g) 275 K. The data are symmetrized along the horizontal axis. Solid lines correspond to the fit according to Eq. (1). The dashed line in panel (g) corresponds to the direction of the uniaxial anisotropy.

model the  $Q(\theta)$  dependence for all temperatures, we applied the following equation, which takes into account both the AEI and uniaxial strain-induced anisotropy [38]:

$$Q = Q_0 \left\{ 1 - \frac{F \sin^2 2\theta}{4J} \right\} - \frac{JZ^2}{8D^3} \sin^4(\theta - \phi). \quad (1)$$

Here  $Z$  represents the uniaxial strain-induced anisotropy constant, and  $\phi$  indicates the corresponding strain-axis direction. The model is similar to the one used for  $\text{Cu}_2\text{OSeO}_3$  [38], with the exception that a term containing the conical angle of the spiral is 0 since the present  $Q(\theta)$  measurements were carried out at zero magnetic field. By applying Eq. (1) to fit the  $Q(\theta)$ -dependent data, we account for the effects of an observed uniaxial distortion and explain its interplay with the AEI in the  $\text{Co}_8\text{Zn}_8\text{Mn}_4$  lamella.

The solid lines in Figs. 3(a)–3(g) represent the  $Q(\theta)$  curves fitted according to Eq. (1). In the fitting procedure, the measured ( $T > 70$  K) or extrapolated according to the power law ( $T < 70$  K) exchange  $J$  and  $D$  constants at each temperature are taken from a previous neutron scattering experiment [34], and the parameters  $Q_0$ ,  $F$ ,  $Z$ , and  $\phi$  adjusted to obtain the best fit to the data. An offset of  $\theta$  and  $\phi$  angles was introduced in the fit to account for the arbitrary sample orientation with respect to the laboratory frame of reference. Remarkably, this simple model including contributions from both the AEI and uniaxial anisotropy provides an excellent agreement with the data and allows for the quantitative extraction of the anisotropic parameters [Figs. 4(b) and 4(c)]. Additional terms including those that are second order in the AEI and the cubic anisotropy do not improve the fit and provide the same fitting results within the experimental error bars.

The temperature dependence of  $Q_0$  obtained from the fitting results shown in Fig. 4(a) agrees well with previous reports from neutron and x-ray scattering experiments [17,30,34,42]. The most important result is shown in Fig. 4(b), where  $F$  is fitted to be negative throughout the entire temperature range and tends to monotonically increase in magnitude toward lower temperatures. From  $F = -0.0036 \pm 0.0015 \text{ pJ m}^{-1}$  at  $T = 275$  K the AEI constant reaches a value of  $F = -0.20 \pm 0.02 \text{ pJ m}^{-1}$  at 20 K. Figure 4(c) shows that the fitted uniaxial anisotropy remains nearly constant across the whole temperature range [Fig. 4(c)], and its contribution to the  $Q$ -vector magnitude is insignificant at low temperature as compared to the AEI. We mention, nevertheless, that the presence of the strain-induced anisotropy offers the possibility of stabilizing a chiral soliton lattice in  $\text{Co}_8\text{Zn}_8\text{Mn}_4$  close to room temperature [42,43].

Our findings provide valuable microscopic insights into the competition between anisotropies in  $\text{Co}_8\text{Zn}_8\text{Mn}_4$  and shed light on their role in determining the magnetic properties, including the unusual temperature variation of the helical wave vector and the transformation of the metastable skyrmion lattice state. Notably,  $|F|$  increases by a factor of four on cooling from 275 K to 20 K, yet this variation alone cannot explain the dramatic change of  $Q_0$  length on cooling, or the persistent helical wave vector alignment with the cubic (100) directions. Instead, the significant temperature dependencies of  $J$  and  $D$  [34], in combination with the cubic anisotropy [24], dominate the observed fundamental behavior of the helical wave vectors and the shape change of the metastable skyrmion lattice [17,28] in  $\text{Co}_8\text{Zn}_8\text{Mn}_4$ , with the underlying AEI playing a minor role. Nonetheless, we note that the AEI can be brought to bear on the observable properties through a suppression

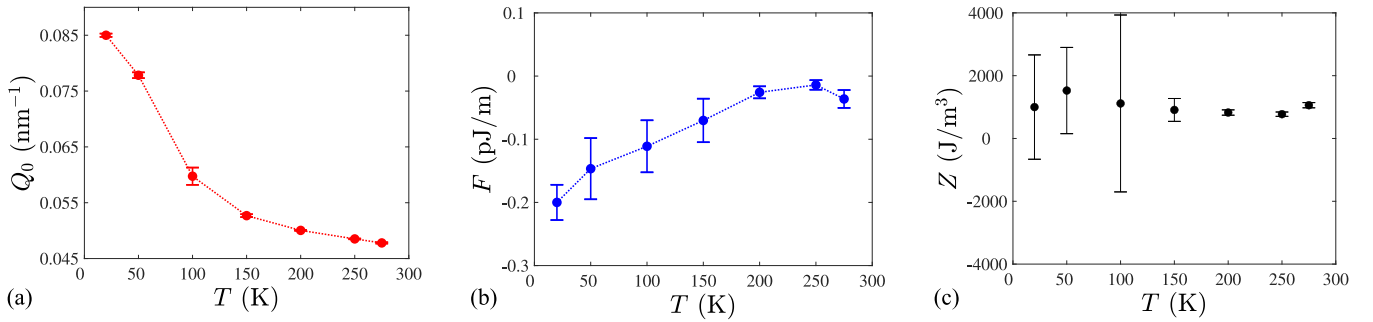


FIG. 4. Temperature dependence of (a) spiral wave vector  $Q_0$ , (b) the exchange anisotropy constant  $F$ , and (c) the strain-induced uniaxial anisotropy constant  $Z$  extracted from the fit of  $Q(\theta)$  according to Eq. (1).

of cubic anisotropy so that it is the AEI that determines the helical wave vector alignment. In Co-Zn-Mn compounds this can be achieved by reducing the Mn content [24]. Indeed, the preferred alignment of the helical wave vectors does eventually change to be along the  $\langle 111 \rangle$  directions in Mn-free  $\text{Co}_{10}\text{Zn}_{10}$  [16]. This suggests that compositional tuning can provide control of the helical wave vector properties in very low Mn content Co-Zn-Mn compounds, through fine-tuning the balance between cubic anisotropy and AEI.

In Fig. 5, we compare the extracted  $F/J$  ratio versus reduced temperature  $T/T_C$  for the cubic chiral magnets FeGe [35],  $(\text{Cu}_{0.98}\text{Zn}_{0.02})_2\text{OSeO}_3$  [41],  $\text{Cu}_2\text{OSeO}_3$  [38], and  $\text{Co}_8\text{Zn}_8\text{Mn}_4$  measured experimentally using neutron or x-ray scattering probes. Importantly, the magnitude of the AEI at low temperatures in  $\text{Co}_8\text{Zn}_8\text{Mn}_4$  is even larger than that in  $\text{Cu}_2\text{OSeO}_3$  [38]. This raises interesting questions concerning why tilted conical and thermal-equilibrium low-temperature skyrmion phases are apparently absent in bulk  $\text{Co}_8\text{Zn}_8\text{Mn}_4$  in contrast to  $\text{Cu}_2\text{OSeO}_3$ , where they are readily observed [13,31]. Understanding the interplay between the relatively large AEI and the cubic magnetocrystalline anisotropy in  $\text{Co}_8\text{Zn}_8\text{Mn}_4$ , as well as their relative size, compared with those found in other chiral magnets is important in terms of clarifying their effect on the stability of different chiral magnetic phases, and requires further theoretical investigations.

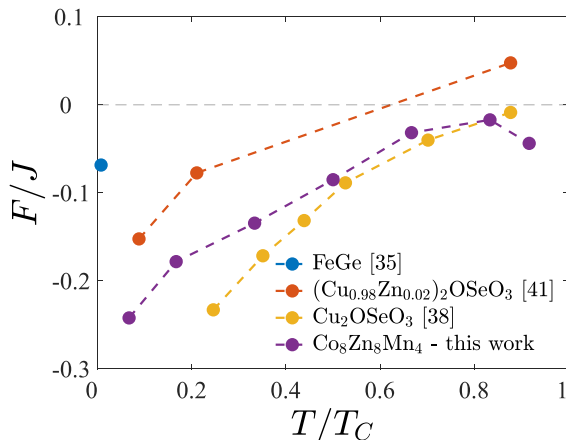


FIG. 5. Comparison between the  $F/J$  ratios vs reduced temperatures for FeGe [35], Zn-doped  $\text{Cu}_2\text{OSeO}_3$  [41], pristine  $\text{Cu}_2\text{OSeO}_3$  [38], and  $\text{Co}_8\text{Zn}_8\text{Mn}_4$  (this work).

The microscopic parameters derived in the present study, along with previous works on the cubic anisotropy [24] and exchange stiffness [34], provide a basis for theoretical models to elucidate the complex magnetic phase diagrams and the stability of exotic magnetic states in  $\text{Co}_8\text{Zn}_8\text{Mn}_4$  at different temperatures and magnetic fields. The Co-Zn-Mn class of chiral magnets challenges the time-honored Bak-Jensen model and calls for inclusion of ingredients that take into account the microscopic richness of these materials, such as short-range magnetic order and frustration-driven fluctuations typical to  $\beta$ -Mn alloys [23,27,44–46]. Such theoretical studies could offer valuable insights into the underlying mechanisms governing the magnetic properties over multiple magnetic length scales in this class of chiral skyrmion hosts.

#### IV. CONCLUSION

In summary, resonant x-ray scattering techniques have been employed to provide new microscopic measurements of the anisotropic exchange interaction (AEI) in the chiral cubic magnet  $\text{Co}_8\text{Zn}_8\text{Mn}_4$ . Applying a theoretical model that incorporates both the AEI and uniaxial strain-induced anisotropy contributions to the data allows for the quantitative extraction of the AEI parameter  $F$ . The observation of a negative value for  $F$  over the entire temperature range below  $T_C$  is at odds with the positive value expected according to the known preferred alignment of the helical wave vector, which itself indicates the existence of an underlying competition between the AEI and a more dominant magnetocrystalline anisotropy on the properties of the helical order in  $\text{Co}_8\text{Zn}_8\text{Mn}_4$ .

Interestingly, despite the comparable magnitude of  $F$  to that of  $\text{Cu}_2\text{OSeO}_3$ , the AEI does not seem to enrich the magnetic phase diagram of  $\text{Co}_8\text{Zn}_8\text{Mn}_4$  with tilted conical and disordered skyrmion phases. Additionally, short-range magnetic order and magnetic fluctuations, which drive the disordered skyrmion phase in the highly frustrated  $\text{Co}_7\text{Zn}_7\text{Mn}_6$ , do not stabilize low-temperature skyrmions in  $\text{Co}_8\text{Zn}_8\text{Mn}_4$  either [23]. However, the chemical tunability of Co-Zn-Mn compounds offers an exciting opportunity for further engineering of magnetic anisotropies and helical structures, potentially enabling the tuning of the skyrmion phase diagram and inducing novel twisted phases in this class of materials.

Overall, this study contributes to the deeper quantitative understanding of the magnetic interactions in  $\text{Co}_8\text{Zn}_8\text{Mn}_4$ , paving the way for future research in this area and opening up possibilities for exploring new magnetic phases and

functionalities in chiral cubic magnets through controlled manipulation of their magnetic anisotropy.

### ACKNOWLEDGMENTS

The authors thank E. Deckardt, M. Bednarzik, and Th. Jung for their help in preparation of the membranes at PSI. The REXS experiment was carried out at the beamline PM-2 VEKMAG at BESSY II synchrotron as a part of Proposal No. 222-11296-ST. We thank the Helmholtz-Zentrum Berlin für Materialien und Energie for the allocation of synchrotron radiation beamtime at both VEKMAG and MAXYMUS. The authors acknowledge funding from JST-CREST (Grant No. JPMJCR20T1). We also acknowledge financial support for

the VEKMAG project and for the PM2-VEKMAG beamline by the German Federal Ministry for Education and Research (BMBF No. 05K2010, No. 05K2013, No. 05K2016, and No. 05K2019) and by HZB. F.R. acknowledges funding by the German Research Foundation via Project No. SPP 2137/RA 3570. O.I.U. acknowledges support from the Institute for Basic Science (IBS) in the Republic of Korea through Project No. IBS-R024-D1. M.W. acknowledges support from the International Max Planck Research School for Chemistry and Physics of Quantum Materials (IMPRS-CPQM), and B.R. is grateful for funding from the DFG through SPP 2137, Project No. 403503416. J.S.W. acknowledges funding from the SNSF Project No. 200021\_188707. K.K. acknowledges funding by the JSPS KAKENHI (Grant No. 23H01841).

- 
- [1] A. Bogdanov and A. Hubert, Thermodynamically stable magnetic vortex states in magnetic crystals, *J. Magn. Magn. Mater.* **138**, 255 (1994).
- [2] N. Nagaosa and Y. Tokura, Topological properties and dynamics of magnetic skyrmions, *Nat. Nanotechnol.* **8**, 899 (2013).
- [3] A. Fert, N. Reyren, and V. Cros, Magnetic skyrmions: Advances in physics and potential applications, *Nat. Rev. Mater.* **2**, 17031 (2017).
- [4] Y. Togawa, Y. Kousaka, S. Nishihara, K. Inoue, J. Akimitsu, A. Ovchinnikov, and J. Kishine, Interlayer magnetoresistance due to chiral soliton lattice formation in hexagonal chiral magnet CrNb<sub>3</sub>S<sub>6</sub>, *Phys. Rev. Lett.* **111**, 197204 (2013).
- [5] N. Kanazawa, Y. Onose, T. Arima, D. Okuyama, K. Ohoyama, S. Wakimoto, K. Kakurai, S. Ishiwata, and Y. Tokura, Large topological Hall effect in a short-period helimagnet MnGe, *Phys. Rev. Lett.* **106**, 156603 (2011).
- [6] S. Mülbauer, B. Binz, F. Jonietz, C. Pfleiderer, A. Rosch, A. Neubauer, R. Georgii, and P. Böni, Skyrmion lattice in a chiral magnet, *Science* **323**, 915 (2009).
- [7] A. K. Nayak, V. Kumar, T. Ma, P. Werner, E. Pippel, R. Sahoo, F. Damay, U. K. Röbber, C. Felser, and S. S. Parkin, Magnetic antiskyrmions above room temperature in tetragonal Heusler materials, *Nature (London)* **548**, 561 (2017).
- [8] Y. Tokura and N. Kanazawa, Magnetic skyrmion materials, *Chem. Rev.* **121**, 2857 (2021).
- [9] I. Dzyaloshinsky, A thermodynamic theory of “weak” ferromagnetism of antiferromagnetics, *J. Phys. Chem. Solids* **4**, 241 (1958).
- [10] T. Moriya, Anisotropic superexchange interaction and weak ferromagnetism, *Phys. Rev.* **120**, 91 (1960).
- [11] P. Bak and M. H. Jensen, Theory of helical magnetic structures and phase transitions in MnSi and FeGe, *J. Phys. C* **13**, L881 (1980).
- [12] S. V. Maleyev, Cubic magnets with Dzyaloshinskii-Moriya interaction at low temperature, *Phys. Rev. B* **73**, 174402 (2006).
- [13] A. Chacon, L. Heinen, M. Halder, A. Bauer, W. Simeth, S. Mühlbauer, H. Berger, M. Garst, A. Rosch, and C. Pfleiderer, Observation of two independent skyrmion phases in a chiral magnetic material, *Nat. Phys.* **14**, 936 (2018).
- [14] L. J. Bannenberg, H. Wilhelm, R. Cubitt, A. Labh, M. P. Schmidt, E. Lelièvre-Berna, C. Pappas, M. Mostovoy, and A. O. Leonov, Multiple low-temperature skyrmionic states in a bulk chiral magnet, *npj Quantum Mater.* **4**, 11 (2019).
- [15] Y. Tokunaga, X. Yu, J. S. White, H. M. Rønnow, D. Morikawa, Y. Taguchi, and Y. Tokura, A new class of chiral materials hosting magnetic skyrmions beyond room temperature, *Nat. Commun.* **6**, 7638 (2015).
- [16] K. Karube, J. S. White, V. Ukleev, C. D. Dewhurst, R. Cubitt, A. Kikkawa, Y. Tokunaga, H. M. Rønnow, Y. Tokura, and Y. Taguchi, Metastable skyrmion lattices governed by magnetic disorder and anisotropy in  $\beta$ -Mn-type chiral magnets, *Phys. Rev. B* **102**, 064408 (2020).
- [17] K. Karube, J. S. White, N. Reynolds, J. Gavilano, H. Oike, A. Kikkawa, F. Kagawa, Y. Tokunaga, Y. Tokura *et al.*, Robust metastable skyrmions and their triangular-square lattice structural transition in a high-temperature chiral magnet, *Nat. Mater.* **15**, 1237 (2016).
- [18] K. Karube, J. S. White, D. Morikawa, M. Bartkowiak, A. Kikkawa, Y. Tokunaga, T. Arima, H. M. Rønnow, Y. Tokura, and Y. Taguchi, Skyrmion formation in a bulk chiral magnet at zero magnetic field and above room temperature, *Phys. Rev. Mater.* **1**, 074405 (2017).
- [19] K. Karube, J. S. White, D. Morikawa, C. D. Dewhurst, R. Cubitt, A. Kikkawa, X. Yu, Y. Tokunaga, T.-h. Arima, H. M. Rønnow *et al.*, Disordered skyrmion phase stabilized by magnetic frustration in a chiral magnet, *Sci. Adv.* **4**, eaar7043 (2018).
- [20] X. Yu, W. Koshibae, Y. Tokunaga, K. Shibata, Y. Taguchi, N. Nagaosa, and Y. Tokura, Transformation between meron and skyrmion topological spin textures in a chiral magnet, *Nature (London)* **564**, 95 (2018).
- [21] T. Nakajima, K. Karube, Y. Ishikawa, M. Yonemura, N. Reynolds, J. S. White, H. M. Rønnow, A. Kikkawa, Y. Tokunaga, Y. Taguchi, Y. Tokura, and T. Arima, Correlation between site occupancies and spin-glass transition in skyrmion host Co<sub>10- $\frac{3}{2}$</sub> Zn<sub>10- $\frac{3}{2}$</sub> Mn<sub>x</sub>, *Phys. Rev. B* **100**, 064407 (2019).
- [22] J. D. Bocarsly, C. Heikes, C. M. Brown, S. D. Wilson, and R. Seshadri, Deciphering structural and magnetic disorder in the chiral skyrmion host materials Co<sub>x</sub>Zn<sub>y</sub>Mn<sub>z</sub> ( $x + y + z = 20$ ), *Phys. Rev. Mater.* **3**, 014402 (2019).
- [23] V. Ukleev, K. Karube, P. Derlet, C. Wang, H. Luetkens, D. Morikawa, A. Kikkawa, L. Mangin-Thro, A. Wildes, Y. Yamasaki *et al.*, Frustration-driven magnetic fluctuations as the

- origin of the low-temperature skyrmion phase in  $\text{Co}_7\text{Zn}_7\text{Mn}_6$ , *npj Quantum Mater.* **6**, 40 (2021).
- [24] M. Preißinger, K. Karube, D. Ehlers, B. Szigeti, H.-A. Krug von Nidda, J. S. White, V. Ukleev, H. M. Rønnow, Y. Tokunaga, A. Kikkawa *et al.*, Vital role of magnetocrystalline anisotropy in cubic chiral skyrmion hosts, *npj Quantum Mater.* **6**, 65 (2021).
- [25] T. Hicken, M. N. Wilson, K. J. A. Franke, B. M. Huddart, Z. Hawkhead, M. Gomilšek, S. J. Clark, F. L. Pratt, A. Štefančič, A. E. Hall *et al.*, Megahertz dynamics in skyrmion systems probed with muon-spin relaxation, *Phys. Rev. B* **103**, 024428 (2021).
- [26] T. Nagase, Y.-G. So, H. Yasui, T. Ishida, H. K. Yoshida, Y. Tanaka, K. Saitoh, N. Ikarashi, Y. Kawaguchi, M. Kuwahara *et al.*, Observation of domain wall bimerons in chiral magnets, *Nat. Commun.* **12**, 3490 (2021).
- [27] J. S. White, K. Karube, V. Ukleev, P. Derlet, R. Cubitt, C. D. Dewhurst, A. Wildes, X. Yu, H. M. Rønnow, Y. Tokura *et al.*, Small-angle neutron scattering study of mesoscale magnetic disordering and skyrmion phase suppression in the frustrated chiral magnet  $\text{Co}_{6.75}\text{Zn}_{6.75}\text{Mn}_{6.5}$ , *J. Appl. Crystallogr.* **55**, 1219 (2022).
- [28] D. Morikawa, X. Yu, K. Karube, Y. Tokunaga, Y. Taguchi, T.-h. Arima, and Y. Tokura, Deformation of topologically-protected supercooled skyrmions in a thin plate of chiral magnet  $\text{Co}_8\text{Zn}_8\text{Mn}_4$ , *Nano Lett.* **17**, 1637 (2017).
- [29] V. Ukleev, Y. Yamasaki, D. Morikawa, K. Karube, K. Shibata, Y. Tokunaga, Y. Okamura, K. Amemiya, M. Valvidares, H. Nakao *et al.*, Element-specific soft x-ray spectroscopy, scattering, and imaging studies of the skyrmion-hosting compound  $\text{Co}_8\text{Zn}_8\text{Mn}_4$ , *Phys. Rev. B* **99**, 144408 (2019).
- [30] M. E. Henderson, M. Bleuel, J. Beare, D. G. Cory, B. Heacock, M. G. Huber, G. M. Luke, M. Pula, D. Sarenac, S. Sharma *et al.*, Skyrmion alignment and pinning effects in the disordered multiphase skyrmion material  $\text{Co}_8\text{Zn}_8\text{Mn}_4$ , *Phys. Rev. B* **106**, 094435 (2022).
- [31] F. Qian, L. J. Bannenberg, H. Wilhelm, G. Chaboussant, L. M. Debeer-Schmitt, M. P. Schmidt, A. Aqeel, T. T. Palstra, E. Brück, A. J. Lefering *et al.*, New magnetic phase of the chiral skyrmion material  $\text{Cu}_2\text{OSeO}_3$ , *Sci. Adv.* **4**, eaat7323 (2018).
- [32] A. O. Leonov and C. Pappas, Reorientation processes of tilted skyrmion and spiral states in a bulk cubic helimagnet  $\text{Cu}_2\text{OSeO}_3$ , *Front. Phys.* **11**, 1105784 (2023).
- [33] S. V. Grigoriev, A. S. Sukhanov, and S. V. Maleyev, From spiral to ferromagnetic structure in B20 compounds: Role of cubic anisotropy, *Phys. Rev. B* **91**, 224429 (2015).
- [34] V. Ukleev, K. A. Pschenichnyi, O. Utesov, K. Karube, S. Mühlbauer, R. Cubitt, Y. Tokura, Y. Taguchi, J. S. White, and S. V. Grigoriev, Spin wave stiffness and damping in a frustrated chiral helimagnet  $\text{Co}_8\text{Zn}_8\text{Mn}_4$  as measured by small-angle neutron scattering, *Phys. Rev. Res.* **4**, 023239 (2022).
- [35] V. Ukleev, O. Utesov, L. Yu, C. Luo, K. Chen, F. Radu, Y. Yamasaki, N. Kanazawa, Y. Tokura, T.-h. Arima *et al.*, Signature of anisotropic exchange interaction revealed by vector-field control of the helical order in a FeGe thin plate, *Phys. Rev. Res.* **3**, 013094 (2021).
- [36] See Supplemental Material at <http://link.aps.org/supplemental/10.1103/PhysRevB.109.184415> for more experimental details and theory.
- [37] T. Noll and F. Radu, The mechanics of the VEKMAG experiment, in *Proceedings, 9th Mechanical Engineering Design of Synchrotron Radiation Equipment and Instrumentation (MEDSI 2016): Barcelona, Spain, September 11–16, 2016* (JACoW, Geneva, 2016), p. 370.
- [38] P. R. Baral, O. I. Utesov, C. Luo, F. Radu, A. Magrez, J. S. White, and V. Ukleev, Direct observation of exchange anisotropy in the helimagnetic insulator  $\text{Cu}_2\text{OSeO}_3$ , *Phys. Rev. Res.* **5**, L032019 (2023).
- [39] D. Nolle, M. Weigand, P. Audehm, E. Goering, U. Wiesemann, C. Wolter, E. Nolle, and G. Schütz, Note: Unique characterization possibilities in the ultra high vacuum scanning transmission x-ray microscope (UHV-STXM) “MAXYMUS” using a rotatable permanent magnetic field up to 0.22 T, *Rev. Sci. Instrum.* **83**, 046112 (2012).
- [40] S. V. Grigoriev, D. Chernyshov, V. Dyadkin, V. Dmitriev, S. V. Maleyev, E. Moskvina, D. Menzel, J. Schoenes, and H. Eckerlebe, Crystal handedness and spin helix chirality in  $\text{Fe}_{1-x}\text{Co}_x\text{Si}$ , *Phys. Rev. Lett.* **102**, 037204 (2009).
- [41] S. Moody, P. Nielsen, M. N. Wilson, D. A. Venero, A. Štefančič, G. Balakrishnan, and P. Hatton, Experimental evidence of a change of exchange anisotropy sign with temperature in Zn-substituted  $\text{Cu}_2\text{OSeO}_3$ , *Phys. Rev. Res.* **3**, 043149 (2021).
- [42] V. Ukleev, Y. Yamasaki, O. Utesov, K. Shibata, N. Kanazawa, N. Jaouen, H. Nakao, Y. Tokura, and T.-h. Arima, Metastable solitonic states in the strained itinerant helimagnet FeGe, *Phys. Rev. B* **102**, 014416 (2020).
- [43] R. Brearton, S. Moody, L. Turnbull, P. Hatton, A. Štefančič, G. Balakrishnan, G. van der Laan, and T. Hesjedal, Observation of the chiral soliton lattice above room temperature, *Adv. Phys. Res.* **2**, 2200116 (2023).
- [44] T. Eriksson, L. Bergqvist, Y. Andersson, P. Nordblad, and O. Eriksson, Magnetic properties of selected mn-based transition metal compounds with  $\beta$ -Mn structure: Experiments and theory, *Phys. Rev. B* **72**, 144427 (2005).
- [45] J. A. Paddison, J. R. Stewart, P. Manuel, P. Courtois, G. J. McIntyre, B. D. Rainford, and A. L. Goodwin, Emergent frustration in Co-doped  $\beta$ -Mn, *Phys. Rev. Lett.* **110**, 267207 (2013).
- [46] H. Yamauchi, D. P. Sari, I. Watanabe, Y. Yasui, L.-J. Chang, K. Kondo, T. U. Ito, M. Ishikado, M. Hagihara, M. D. Frontzek *et al.*, High-temperature short-range order in  $\text{Mn}_3\text{RhSi}$ , *Commun. Mater.* **1**, 43 (2020).